Nuclear Instruments and Methods in Physics Research B 359 (2015) 69–74

Contents lists available at ScienceDirect

Nuclear Instruments and Methods in Physics Research B

journal homepage: www.elsevier.com/locate/nimb

Effects of helium and hydrogen on radiation-induced microstructural changes in austenitic stainless steel

Hyung-Ha Jin *, Eunsol Ko, Sangyeop Lim, Junhyun Kwon

Nuclear Materials Safety Research Division, Korea Atomic Energy Research Institute, 989-111 Daedeok-daero, Yuseong-gu, Daejeon 305-353, Republic of Korea

ARTICLE INFO

Article history:
Received 11 May 2015
Received in revised form 3 July 2015
Accepted 16 July 2015
Available online 28 July 2015

Keywords:
Radiation induced microstructural changes
Ion irradiation
TEM analysis
Segregation
Defect

ABSTRACT

Microstructural changes in austenitic stainless steel by helium, hydrogen, and iron ion irradiation were investigated with transmission electron microscopy. Typical radiation-induced changes, such as the formation of Frank loops in the matrix and radiation-induced segregation (RIS) or depletion at grain boundaries, were observed after ion irradiation. The helium ion irradiation led to the formation of cavities both at grain boundaries and in the matrix, as well as the development of smaller Frank loops. The hydrogen ion irradiation generated stronger RIS behavior at the grain boundaries compared to irradiation with helium and iron ions. The effects of helium and hydrogen on radiation-induced microstructural changes were discussed.

1. Introduction

Stress corrosion cracking (SCC) by neutron irradiation is a significant concern for materials used in commercial nuclear reactors under extended operation [1–3]. Irradiation-assisted stress corrosion cracking (IASCC) is known to be closely related to microstructural changes caused by radiation, such as the formation of defects in the metallic matrix and the development of radiation-induced segregation (RIS) at grain boundaries, which depletes chromium and enriches nickel, silicon, and phosphorus. The depletion of chromium at grain boundaries was thought to be identified as a primary factor for IASCC susceptibility in commercial boiling-water nuclear reactors (BWR) [4]. However, the RIS phenomenon at the grain boundary was recognized as a supplementary or minor factor for affecting IASCC susceptibility in pressurized-water nuclear reactors (PWR) [3,5,6]. Localized deformation behavior by the existence of radiation defects is possibly a strong contributor to IASCC. Localized deformation is known to promote dislocation pileups at grain boundaries, resulting in the initiation of SCC via the rupture of the surface oxide film [7,8]. Recently, the retention of helium and hydrogen was identified as another possible factor affecting the IASCC susceptibility of nuclear internals [9,10]. In one experiment [9], austenitic stainless steels irradiated in a PWR had higher hydrogen (3500 appm)/helium (600 appm) gas concentrations and lower IASCC susceptibilities compared to those irradiated in a fast breeder reactor (FBR). Based on these experimental results, it was proposed that hydrogen and helium may also affect the IASCC susceptibility of PWR core internal materials, in addition to RIS formation and radiation-induced hardening behavior.

The effect of helium irradiation on radiation-induced defect microstructures and the corresponding hardening behavior in austenitic stainless steel were investigated by Lee et al. [11–13] and Hunn et al. [14]. These studies revealed that additional helium-induced hardening developed due to the formation of helium-filled cavities. Helium bubbles were found to dramatically affect the evolution of radiation-induced microstructures. These investigations focused on the effect of helium on the evolution of radiation defects and the changes in mechanical properties resulting from a certain radiation environment that produces considerable quantities of transmutation products, such as hydrogen and helium.

In this work, we provide additional information on the effects of helium and hydrogen on the evolution of RIS, as well as radiation defects in austenitic stainless steel. We characterize the microstructure of austenitic stainless steels irradiated with helium, hydrogen, and iron ions. Transmission electron microscopy (TEM) was used to characterize the microstructural changes in these irradiated metal samples.

2. Experimental

Commercial SS316 austenitic stainless steel was used for this work, with a composition by weight of 10.8% nickel, 16.7%

* Corresponding author. Tel.: +82 42 868 4790; fax: +82 42 868 8549.
E-mail address: hhajin2@kaeri.re.kr (H.-H. Jin).

http://dx.doi.org/10.1016/j.nimb.2015.07.086
0168-583X/

chromium, 2.0% molybdenum, 1.3% manganese, 0.047% carbon, and 0.59% silicon, with the balance in iron. As impurities, 0.05% phosphorus and 0.001% sulfur were present. Mechanical polishing was performed using suspensions of diamond with sizes of 3 μm and 0.25 μm. Fine polishing was performed with a vibratory polisher (Vibromet 2) using colloidal silica (0.02 μm) to minimize any surface damage generated in the previous polishing steps.

Ion irradiation experiments were performed using a multi-purpose ion implanter at the Korea Institute of Geoscience & Mineral Resources (KIGAM). Helium ions (He^+) or hydrogen ions (H_2^+) were used in multiple energies ranges, from 490 keV to 50 or 100 keV, for the development of uniform radiation damage (5 displacements per atom, or dpa) and implanted ion concentrations in the ion-irradiated samples. Another ion irradiation was performed using a Tandem ion accelerator with 8 MeV iron ions (Fe^{4+}). The ion energies and fluences for all ion irradiation experiments are shown in Table 1. The irradiation temperature was set to 400 °C. Fig. 1 shows the radiation damage profile and concentration of residual implanted ions after irradiations with helium and hydrogen ion, calculated by the Stopping Range of Ions and Matter (SRIM) computer program [15,16]. The radiation damage profile resulting from the single iron irradiation is also displayed in Fig. 1(c).

Since the ion-irradiated layers were calculated to be approximately 1–2 μm in depth, depending on the irradiation media, as shown in Fig. 1, a focused ion beam (FIB) technique was applied to fabricate cross-sectional TEM samples from selected regions in the ion-irradiated layer. The TEM lamellae were treated with a low-energy Ar-ion milling after the high-energy Ga-ion milling with FIB [17].

A TEM (JEOL 2100F) equipped with an energy-dispersive spectrometry (EDS) system was used to analyze radiation-induced defects and RIS at the grain boundaries of the steel samples. To minimize the effect of specimen drift under EDS analysis, the site-lock option available in the EDS system (INCA, Oxford) was used during the analysis. To measure the thickness of the TEM samples to quantify the results of radiation defects, electron energy loss spectroscopy (EELS) was conducted during the TEM observation. Most researchers have used the reciprocal lattice rod (rel-rod) dark-field imaging method to quantify Frank loops observed in irradiated austenitic stainless steels. However, TEM bright-field and high-resolution imaging was used to analyze Frank loops in this work, because of the thinner radiation damage layer present in the TEM sample. Out-of-focus contrast condition was used to observe small cavities. We also conducted the inside–outside contrast technique in order to determine the nature of dislocation loop [18].

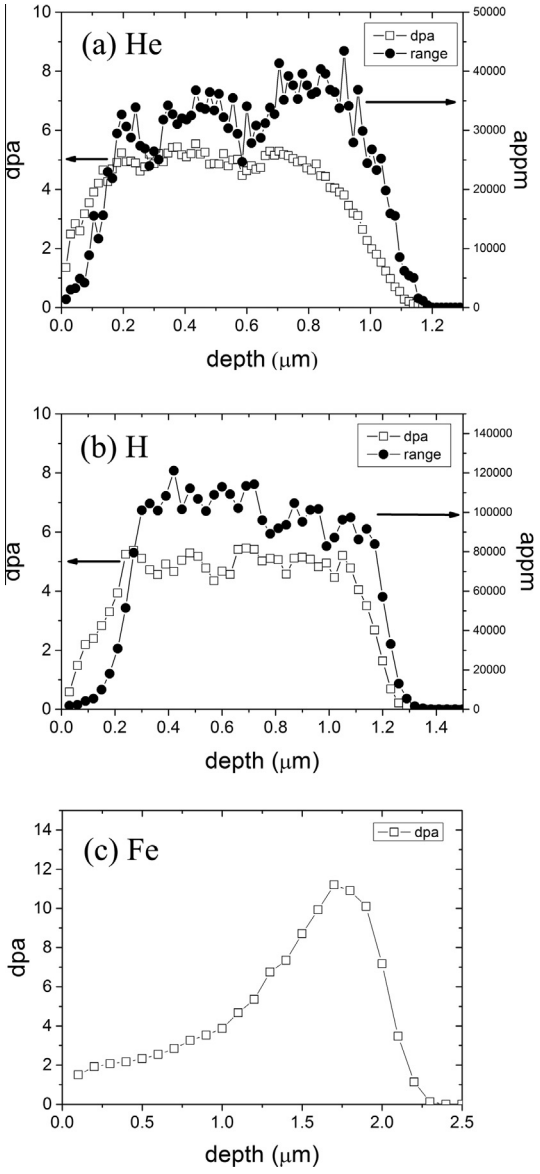

Fig. 1. Radiation-induced damage and residual implanted ion concentration introduced by ion bombardment as a function of depth, calculated with SRIM [15]. A displacement energy of 40 eV was used for the calculation [16]. The calculation was performed in full cascade mode.

3. Results and discussion

Low-magnification TEM images of the irradiated austenitic stainless steels are shown in Fig. 2. Radiation damage is present uniformly up to a depth of approximately 1 μm in the helium-implanted sample. The experimentally measured depth of the radiation damage is similar to that calculated by SRIM. In the case of hydrogen implantation, the radiation damage seems to be formed up to a depth of approximately 0.8 μm, somewhat less than

Table 1
Ion energies and corresponding fluences.

		1	2	3	4	5	6	7	8	9
He	Energy (keV)	490	400	300	200	150	100	50		
	Fluence (ion/cm^2)	5E16	5E16	5E16	3E16	3E16	3E16	3E16		
	Dose rate (dpa/s)	~2.5E-4								
H	Energy (keV)	490	450	400	350	300	250	200	150	100
	Fluence (ion/cm^2)	7E16	4E16	5E16	4E16	17E16	9E16	4E16	5E16	4E16
	Dose rate (dpa/s)	~4.2E-4								
Fe	Energy(keV)	8000								
	Fluence (ion/cm^2)	5.8E15								
	Dose rate (dpa/s)	~3.5E-4 (at a depth of 1 μm)								